Bulg. J. Phys. **42** (2015) 172–199

Excitonic and Vibronic Spectra of Two-Dimensional Symmetric Donor–Acceptor Lattices

I. J. Lalov, **I. Zhelyazkov**
Faculty of Physics, University of Sofia, 1164 Sofia, Bulgaria

Received *30 April 2015*

Abstract. The excitonic and vibronic spectra of quadratic and hexagonal two-dimensional (2D) lattices of regularly arranged donor and acceptor molecules and the manifestation of those spectra in the linear absorption are modeled and numerically simulated. The splitting of the spectra caused by Frenkel excitons (FEs) and charge-transfer excitons (CTEs) coupling as well as by the anisotropy of the model has been studied analytically and displayed by simulations. The excitonic density of states, their renormalization by the FE–CTEs coupling and the shape of absorption lines in the excitonic, one-phonon, and two-phonon vibronic spectra have been calculated. The main results can be used in interpreting the absorption spectra of 2D symmetric donor–acceptor lattices.

PACS codes: 71.35.Aa, 71.35.Cc, 71.35.Pq

1 Introduction

Donor–acceptor (DA) systems represent a big part of charge-transfer (CT) solids and exhibit promising linear and nonlinear properties (see [1], Ch. 11). Their studies began a half century ago initially associated with the spectra of their electronic excitations. The lowest excited electronic state could be a charge-transfer exciton (CTE) with the electron on the ionized acceptor and the hole on the neighboring donor or could be a mixed CT and Frenkel exciton. The excitonic spectra and their vibronic replicas strongly influence the linear [2–6] and nonlinear [7] properties of the CT systems.

The most widely known DA crystal is the anthracene-PMDA [2–4, 8–10] whose excitonic spectrum is described on the basis of the model of one-dimensional molecular stack with regularly and alternatively arranged DA molecules. We used the same 1D model in our theoretical studies of excitonic and vibronic spectra [11,12]. In the present paper, we consider a two-dimensional (2D) model of regularly arranged DA molecules, which create a plane quadratic or hexagonal lattice. The model of a quadratic 2D lattice has been analyzed by using Ising models in statistical mechanics [13, 14]. Donor–acceptor crystals can be treated

as a binary system at low temperatures with an alternating ordering of donor and acceptor molecules. In our study, we stress on the theoretical model of a high-symmetry 2D system with a strong anisotropy of the linear absorption in directions parallel to the lattice plane and perpendicular to it [15, 16]. Such type of a DA system is not realized experimentally but obviously the complex coupling of Frenkel excitons (FEs), CTEs, and the intramolecular vibrations should be the right model of the excitonic and vibronic spectra of 2D symmetric structures.

In the case of a quadratic lattice with one donor and one acceptor molecule in unit cell, four CTEs branches can describe the electron–hole pairs in the neighbor molecules and they represent physically equivalent quasiparticles (by using their indentity in the case of a 90°-rotation). In our model, we include the opportunity of mutual transformations of those four CTEs branches caused by the transfer of an electron or a hole on the closest positions of acceptors and donors, respectively. These transfers ensure the mobility of CTEs. The geometry of our hexagonal 2D donor–acceptor lattice is a graphene-like with two different entities in the unit cell [17]. Three nearest acceptor molecules are neighbors of each donor molecule and thus three physically equivalent CTEs must be included in the analysis of the excitonic spectra.

We consider the mixing of CTEs and FEs. The electronic excited state of a FE stems from the excitation of a neutral donor (the case of FEs originating from the excitation of acceptors is completely analogous). Frenkel excitons are mobile, too, via the transfer of the excitation on the neighbor neutral donor. The FEs–CTEs coupling is accomplished through the transfer of FE's electron to the one of the neighbor acceptor molecules (and vice verse). The intramolecular vibration coupled linearly with a mixed FE–CTEs can be both vibrational mode of the donor or of the acceptor molecule. In the paper, the linear optical susceptibility, χ, is calculated by using the Green function formalism (at $T = 0$) and the vibronic approach [18] for the excitonic and one-phonon vibronic regimes. The calculations of χ and the linear absorption coefficient have been done separately for the case of light whose electric vector is perpendicular to the quadratic lattice plane and parallel to it.

This paper, consists of two parts: Part A in which we study the excitonic and vibronic spectra of a quadratic 2D donor–acceptor (DA) lattice. In the next section, we introduce the theoretical model and calculate the χ_{zz} component for light polarized normally to the plane. In Section 3, the $\chi_{xx} = \chi_{yy}$ components of light's electric vector parallel to the crystal plane are found taking into account the FE–CTEs coupling inside the plane of the layer. In Section 4, we perform numerical calculations of the excitonic densities of states (DOSs) and the absorption coefficient for both polarizations. In Part B we explore excitons in a hexagonal graphene-like DA lattice. Sections 5 and 6 are devoted to the theoretical treatment of the excitons and vibronic spectra, and Sect. 7 contains the results of their numerical simulations. Section 8 represents a conclusion and an outlook for the excitonic and vibronic spectra manifestation.

Part A: Excitons in a Quadratic 2D Donor–Acceptor Lattice

2 Linear Optical Susceptibility in a Direction Perpendicular to a Quadratic Lattice

Let us consider a quadratic 2D lattice with a distance a between the neighbour nodes where the donor molecules are located (see Figure 1). We suppose that the acceptor molecules occupy the centres of the unit cells and CTEs represent the neighbor DA pairs. By introducing the operators of annihilation, $C_{i,nm}$, where $i = 1$–4, nm is the node of the ionized donor, the CTE's part of the Hamiltonian has the form [15]:

$$\begin{aligned}\hat{H}_{\mathrm{CTE}} = & \sum_{nm,\, i=1\text{–}4} E_{\mathrm{c}} C^{+}_{i,nm} C_{i,nm} + \sum_{nm} J_{\mathrm{e}} \Big[C^{+}_{2,nm} C_{1,nm} \\ & + C^{+}_{3,nm} C_{2,nm} + C^{+}_{4,nm} C_{3,nm} + C^{+}_{1,nm} C_{4,nm} + \mathrm{h.c.} \Big] \\ & + \sum_{nm} J_{\mathrm{h}} \Big[C^{+}_{2,n+1\,m} C_{1,nm} + C^{+}_{3,n\,m+1} C_{2,nm} \\ & + C^{+}_{4,n-1\,m} C_{3,nm} + C^{+}_{1,n\,m-1} C_{4,nm} + \mathrm{h.c.} \Big], \end{aligned} \tag{1}$$

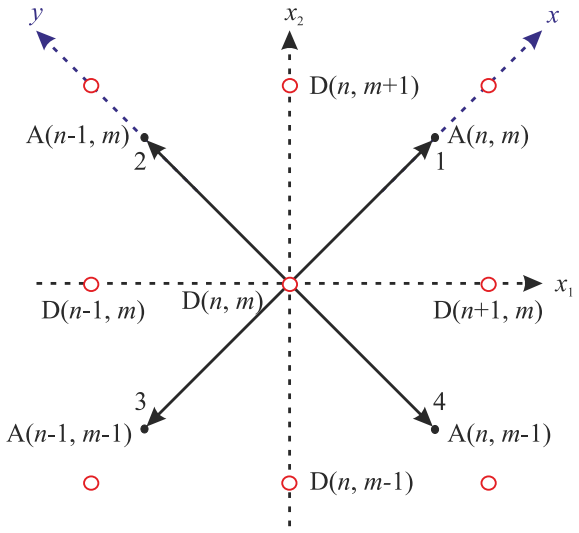

Figure 1. Two-dimensional donor–acceptor quadratic lattice. The donor molecules are positioned at the nodes of the lattice whereas the acceptor molecules occupy the centres of the quadratic unit cells. Numerals 1–4 denote the numbers of CTEs.

where $E_{\rm c}$ is the excitation energy of all CTEs, $J_{\rm e}$ is the transfer integral of the electron between the neighbor acceptor molecules, and $J_{\rm h}$ is the transfer integral of the hole between the neighbor donors. By using the Fourier-components of the CTEs operators in momentum space $\boldsymbol{k} = (k_1, k_2)$, we obtain:

$$\hat{H}_{\rm CTE} = \sum_{\boldsymbol{k},\, i=1\text{–}4} \Big\{ E_{\rm c} C^{+}_{i\boldsymbol{k}} C_{i\boldsymbol{k}} + J_{\rm e} \Big[C^{+}_{2\boldsymbol{k}} C_{1\boldsymbol{k}} + C^{+}_{3\boldsymbol{k}} C_{2\boldsymbol{k}} + C^{+}_{4\boldsymbol{k}} C_{3\boldsymbol{k}} + C^{+}_{1\boldsymbol{k}} C_{4\boldsymbol{k}} + \text{h.c.} \Big] + J_{\rm h} \Big[C^{+}_{4\boldsymbol{k}} C_{1\boldsymbol{k}} \mathrm{e}^{-\mathrm{i}k_2 a} + C^{+}_{1\boldsymbol{k}} C_{2\boldsymbol{k}} \mathrm{e}^{\mathrm{i}k_1 a} + C^{+}_{2\boldsymbol{k}} C_{3\boldsymbol{k}} \mathrm{e}^{\mathrm{i}k_2 a} + C^{+}_{3\boldsymbol{k}} C_{4\boldsymbol{k}} \mathrm{e}^{-\mathrm{i}k_1 a} + \text{h.c.} \Big] \Big\}. \quad (2)$$

In this section, we study the coupling of CTEs with those FEs whose transition dipole moment $\boldsymbol{p}$ is perpendicular to the layer. The corresponding part of the Hamiltonian in the nearest neighbors approximations can read as [16]:

$$\hat{H}_{\rm FE} = \sum_{n,m} E_{\rm F} B^{+}_{nm} B_{nm} + W \sum_{n,m} \Big\{ \Big[B^{+}_{n+1,m} + B^{+}_{n-1,m} + B^{+}_{n,m+1} + B^{+}_{n,m-1} \Big] B_{nm} + \text{h.c.} \Big\} = \sum_{\boldsymbol{k}} E_{\rm F}(\boldsymbol{k}) B^{+}_{\boldsymbol{k}} B_{\boldsymbol{k}}, \quad (3)$$

where $E_{\rm F}$ is the excitation energy of FE, W is its transfer integral, and

$$E_{\rm F}(\boldsymbol{k}) = E_{\rm F} + 2W \left[\cos(k_1 a) + \cos(k_2 a) \right]. \quad (4)$$

Obviously, the FE–CTEs coupling can be accomplished via the transfer of an electron from a neutral excited donor (with a FE on it) to the four neighbor acceptors. The coupling part of the Hamiltonian takes the form [12]:

$$\hat{H}_{\text{FE–CTEs}} = \varepsilon \sum_{nm,\, i=1\text{–}4} (C^{+}_{i,nm} B_{nm} + \text{h.c.}) = \varepsilon \sum_{\boldsymbol{k},\, i=1\text{–}4} (C^{+}_{i,\boldsymbol{k}} B_{\boldsymbol{k}} + \text{h.c.}). \quad (5)$$

The mode of intramolecular vibration coupled with FE–CTEs can be vibration of a donor or an acceptor molecule and the following phonon and phonon–exciton linear coupling part appear [12]:

(a) phonon on donors

$$\hat{H}_{\text{ph–d}} = \hbar\omega_0 \sum_{nm,\, i=1\text{–}4} \Big[a^{+}_{nm} a_{nm} + \xi C^{+}_{i,nm} C_{i,nm} (a^{+}_{nm} + a_{nm}) + \xi_{\rm F} B^{+}_{nm} B_{nm} (a^{+}_{nm} + a_{nm}) \Big], \quad (6)$$

where ω_0 is the vibrational frequency, a_{nm} is the annihilation operator of one vibrational quantum on the molecule (nm), and ξ and $\xi_{\rm F}$ are the dimensionless

parameters of the linear exciton–phonon coupling. The linear coupling terms in above equations can be eliminated using the canonical transformation [12]

$$\hat{H}_1 = \exp(Q)\left(\hat{H}_{\mathrm{CTE}} + \hat{H}_{\mathrm{FE}} + \hat{H}_{\mathrm{FE\text{–}CTEs}} + \hat{H}_{\mathrm{ph\text{–}d}}\right)\exp(-Q), \tag{7}$$

in which

$$Q = \sum_{nm,\, i=1\text{–}4} \left[\xi C^{+}_{i,nm} C_{i,nm} + \xi_{\mathrm{F}} B^{+}_{nm} B_{nm}\right]\left(a^{+}_{nm} - a_{nm}\right). \tag{8}$$

We introduce transformed operators

$$U_{i,\boldsymbol{k}} = \exp(Q) C_{i,\boldsymbol{k}} \exp(-Q), \tag{9a}$$

$$V_{\boldsymbol{k}} = \exp(Q) B_{\boldsymbol{k}} \exp(-Q). \tag{9b}$$

In calculating the linear optical susceptibility, we need the operator of the transition dipole moment which is the sum of the transition dipole moments of FEs ($p_{\mathrm{F}z}$) and of CTEs ($p_{\mathrm{c}z}$), notably

$$\begin{aligned} \hat{P} &= \sum_{nm,\, i=1\text{–}4} \left(p_{\mathrm{F}z} V_{nm} + p_{\mathrm{c}z} U_{i,nm} + \mathrm{h.c.}\right) \\ &= p_{\mathrm{F}z} V_{\boldsymbol{k}=0} + p_{\mathrm{c}z} \sum_{i=1\text{–}4} U_{i,\boldsymbol{k}=0} + \mathrm{h.c.} \end{aligned} \tag{10}$$

The transition dipole moment of the CTE, $\boldsymbol{p}_{\mathrm{c}i}$, is directed nearby along the vector joining the centers of the two ions involved [19]. Thus, its component $p_{\mathrm{c}z}$ perpendicular to the plane is very small.

(b) phonon on acceptors

$$\hat{H}_{\mathrm{ph\text{–}a}} = \hbar\omega_1 \sum_{nm,\, i=1\text{–}4} \left[a^{+}_{nm} a_{nm} + \xi_{\mathrm{a}} C^{+}_{i,nm} C_{i,nm} (a^{+}_{(nm)+\sigma_i} + a_{(nm)+\sigma_i})\right] \tag{11}$$

with the analogous of the case (a) symbols ω_1 and ξ_{a}, whereas σ_i denotes the precise place of the CTE's acceptor with $i = 1$–4. Then the canonical transformation (7) becomes simpler and the quantity Q_{a} reads

$$Q_{\mathrm{a}} = \xi_{\mathrm{a}} \sum_{nm,\, i=1\text{–}4} C^{+}_{i,nm} C_{i,nm} \left(a^{+}_{(nm)+\sigma_i} - a_{(nm)+\sigma_i}\right). \tag{12}$$

(Formulas (9) and (10) are valid in the case (b), too.)

In calculating the linear optical susceptibility, χ_{ij}, the following formulas have been used [1, 20]:

$$\chi_{ij} = \lim_{\varepsilon \to +0} \left\{ -\frac{1}{2\hbar V} \left[\Phi_{ij}(\omega + i\varepsilon) + \Phi_{ij}(-\omega + i\varepsilon)\right] \right\} \tag{13}$$

with

$$\Phi_{ij}(t) = -i\theta(t)\langle 0|\hat{P}_i(t)\hat{P}_j(0) + \hat{P}_j(t)\hat{P}_i(0)|0\rangle, \tag{14}$$

where V is the volume of the crystal (layer), and $\hat{P}$ is the operator of the transition dipole moment. The Green functions (14) have been calculated as an average over only the ground state $|0\rangle$ taking into account the large values of E_{F} and $\hbar\omega_0/\hbar\omega_1$ compared with $k_{\mathrm{B}}T$. In calculating the Green functions, we apply the vibronic approach [18] which is valid in the conditions

$$|J_{\mathrm{e}}|, |J_{\mathrm{h}}|, |\varepsilon|, |W| \ll \hbar\omega_0, \hbar\omega_1, E_{\mathrm{F}}, E_{\mathrm{c}}. \tag{15}$$

The calculations are valid correspondingly for pure excitonic spectra ($\hbar\omega \approx E_{\mathrm{F}}, E_{\mathrm{c}}$) or for first vibronic replicas ($\hbar\omega \approx E_{\mathrm{F}} + \hbar\omega_0, E_{\mathrm{c}} + \hbar\omega_0$), etc.

2.1 Excitonic spectra

In calculating the χ_{zz} component, we need the Green function

$$g_{\mathrm{F}}^{(0)}(t) = -\mathrm{i}\theta(t)\langle 0|V_{\boldsymbol{k}=0}(t)V_{\boldsymbol{k}=0}^{+}(0)|0\rangle. \tag{16}$$

Function (16) is coupled via operator (5) with the Green functions

$$g_i^{(0)}(t) = -\mathrm{i}\theta(t)\langle 0|U_{i,\boldsymbol{k}=0}(t)V_{\boldsymbol{k}=0}^{+}(0)|0\rangle, \tag{17}$$

where $i = 1$–4. Due to the symmetry of the quadratic lattice, we obtain for the Fourier components of functions (17)

$$g_1^{(0)} = g_2^{(0)} = g_3^{(0)} = g_4^{(0)}, \tag{18}$$

and the following set of equations holds

$$(\hbar\omega - E_{\mathrm{F}} - 4W - \hbar\omega_{0\mathrm{F}})\, g_{\mathrm{F}}^{(0)} - 4\varepsilon g_1^{(0)} = 1, \tag{19a}$$

$$(\hbar\omega - E_{\mathrm{c}} - 2J - \hbar\omega_{0\mathrm{c}})\, g_1^{(0)} - \varepsilon g_{\mathrm{F}}^{(0)} = 0, \tag{19b}$$

where $J = J_{\mathrm{e}} + J_{\mathrm{h}}$ and $\omega_{0\mathrm{F}}$ and $\omega_{0\mathrm{c}}$ are given by the continuous fractions

$$\omega_{0\mathrm{F}} = \cfrac{\omega_{\mathrm{F}}^2}{\omega - E_{\mathrm{F}}/\hbar - \omega_0 - \cfrac{2\omega_{\mathrm{F}}^2}{\omega - E_{\mathrm{F}}/\hbar - 2\omega_0 - \cfrac{3\omega_{\mathrm{F}}^2}{\cdots}}}, \tag{20a}$$

$$\omega_{0\mathrm{c}} = \cfrac{\omega_{\mathrm{a}}^2}{\omega - E_{\mathrm{c}}/\hbar - \omega_0 - \cfrac{2\omega_{\mathrm{a}}^2}{\omega - E_{\mathrm{c}}/\hbar - 2\omega_0 - \cfrac{3\omega_{\mathrm{a}}^2}{\cdots}}}, \tag{20b}$$

in which $\omega_{\rm F} = \xi_{\rm F}\omega_0$ and $\omega_{\rm a} = \xi\omega_0$ (in the case (b) we have $\xi_{\rm F} = 0$ and $\omega_{\rm a} = \xi_{\rm a}\omega_1$, i.e., ω_1 instead of ω_0).

The same procedure of calculations yields the Fourier components of the Green functions with the operator $\sum_{i=1\text{–}4} U^{+}_{i,\boldsymbol{k}=0}(0)$. The final expression for the χ_{zz} component is

$$\chi_{zz} = -\frac{p^2_{{\rm F}z}\alpha_{22} + 8p_{{\rm F}z}p_{{\rm c}z}\alpha_{12} + 4p^2_{{\rm c}z}\alpha_{11}}{v\left(\alpha_{11}\alpha_{22} - 4\alpha^2_{12}\right)}, \tag{21}$$

in which

$$\alpha_{11} = \hbar(\omega - \omega_{0{\rm F}}) - E_{\rm F} - 4W, \;\; \alpha_{12} = \varepsilon, \;\; \alpha_{22} = \hbar(\omega - \omega_{0{\rm c}}) - E_{\rm c} - 2J, \tag{22}$$

and v is the volume of one elementary cell.

2.2 First vibronic replica

Near the frequencies of the first vibronic replica, $\hbar\omega \approx E_{\rm F} + \hbar\omega_0 \approx E_{\rm c} + \hbar\omega_0$, the set of equations (19) is transformed into the following set:

$$(\hbar\omega - E_{\rm F} - 4W)g^{(0)}_{\rm F} - \hbar\omega_{\rm F}S_{\rm F} - 4\varepsilon g^{(0)}_1 = 1, \tag{23a}$$

$$(\hbar\omega - E_{\rm c} - 2J)g^{(0)}_1 - \hbar\omega_{\rm a}S_1 - \varepsilon g^{(0)}_{\rm F} = 0, \tag{23b}$$

where

$$S_{\rm F} = \sum_{\boldsymbol{k}} g^{(1)}_{\rm F}(\boldsymbol{k}), \quad S_1 = \sum_{\boldsymbol{k}} g^{(1)}_1(\boldsymbol{k}), \tag{24}$$

while $g^{(1)}_{\rm F}(\boldsymbol{k})$ and $g^{(1)}_1(\boldsymbol{k})$ are given by the following Green functions:

$$g^{(1)}_{\rm F}(\boldsymbol{k},t) = -{\rm i}\theta(t)\langle 0|a_{-\boldsymbol{k}}(t)V_{\boldsymbol{k}}(t)V^{+}_{\boldsymbol{k}=0}(0)|0\rangle, \tag{25a}$$

$$g^{(1)}_i(\boldsymbol{k},t) = -{\rm i}\theta(t)\langle 0|a_{-\boldsymbol{k}}(t)U_{i,\boldsymbol{k}}(t)V^{+}_{\boldsymbol{k}=0}(0)|0\rangle, \tag{25b}$$

with $i = 1\text{–}4$ ($a_{\boldsymbol{k}}$ is the Fourier transform in the momentum space of operators a_{nm}). Following the vibronic approach [18], we obtain a set of equations for their Fourier transforms

$$\hbar\omega_{1{\rm F}}(\boldsymbol{k})g^{(1)}_{\rm F}(\boldsymbol{k}) - \varepsilon\sum_{i=1\text{–}4} g^{(1)}_i(\boldsymbol{k}) = \hbar\omega_{\rm F}g^{(0)}_{\rm F} + M_{\rm F}S_{\rm F}, \tag{26}$$

$$\hbar\omega_{1{\rm c}}g^{(1)}_1(\boldsymbol{k}) - \left(J_{\rm e} + J_{\rm h}{\rm e}^{{\rm i}k_1a}\right)g^{(1)}_2(\boldsymbol{k}) - \left(J_{\rm e} + J_{\rm h}{\rm e}^{{\rm i}k_2a}\right)g^{(1)}_4(\boldsymbol{k}) - \varepsilon g^{(1)}_{\rm F}(\boldsymbol{k}) = \hbar\omega_{\rm a}g^{(0)}_1 + MS^{(1)}_1, \tag{27}$$

where

$$\hbar\omega_{1{\rm F}}(\boldsymbol{k}) = \hbar\left(\omega - \omega_0 - \Omega_{1{\rm F}}\right) - E_{\rm F}(\boldsymbol{k}), \tag{28a}$$

$$\hbar\omega_{1{\rm c}} = \hbar\left(\omega - \omega_0 - \Omega_{1{\rm c}}\right) - E_{\rm c}, \tag{28b}$$

while $\omega_{1\mathrm{F}}$ and $\omega_{1\mathrm{c}}$ are the following continuous fractions:

$$\Omega_{1\mathrm{F}} = \cfrac{\omega_{\mathrm{F}}^2}{\omega - E_{\mathrm{F}}/\hbar - 2\omega_0 - \cfrac{2\omega_{\mathrm{F}}^2}{\omega - E_{\mathrm{F}}/\hbar - 3\omega_0 - \cfrac{3\omega_{\mathrm{F}}^2}{\cdots}}}, \tag{29a}$$

$$\Omega_{1\mathrm{c}} = \cfrac{\omega_{\mathrm{a}}^2}{\omega - E_{\mathrm{c}}/\hbar - 2\omega_0 - \cfrac{2\omega_{\mathrm{a}}^2}{\omega - E_{\mathrm{c}}/\hbar - 3\omega_0 - \cfrac{3\omega_{\mathrm{a}}^2}{\cdots}}}, \tag{29b}$$

Functions M_{F} and M can be presented in the following way:

$$M_{\mathrm{F}} = \cfrac{2\omega_{\mathrm{F}}^2}{\omega - E_{\mathrm{F}}/\hbar - 2\omega_0 - \cfrac{3\omega_{\mathrm{F}}^2}{\omega - E_{\mathrm{F}}/\hbar - 3\omega_0 - \cfrac{4\omega_{\mathrm{F}}^2}{\cdots}}} - \Omega_{1\mathrm{F}}\ , \tag{30a}$$

$$M = \cfrac{2\omega_{\mathrm{a}}^2}{\omega - E_{\mathrm{c}}/\hbar - 2\omega_0 - \cfrac{3\omega_{\mathrm{a}}^2}{\omega - E_{\mathrm{c}}/\hbar - 3\omega_0 - \cfrac{4\omega_{\mathrm{a}}^2}{\cdots}}} - \Omega_{1\mathrm{c}}\ . \tag{30b}$$

Equations analogous to (27) can be written for the Green functions $g_2^{(1)}(\boldsymbol{k})$, $g_3^{(1)}(\boldsymbol{k})$, and $g_4^{(1)}(\boldsymbol{k})$. After some algebra, we rederive formula (21) with the following expressions for α_{11}, α_{12}, and α_{22}:

$$\alpha_{11} = \hbar\omega - E_{\mathrm{F}} - 4W - \hbar^2\omega_{\mathrm{F}}^2\left[S_0 + M\left(4S_2^2\varepsilon^2 - S_0S_3\right)\right]/D_2, \tag{31a}$$

$$\alpha_{22} = \hbar\omega - E_{\mathrm{c}} - 2J - \hbar^2\omega_{\mathrm{a}}^2\left[S_3 + M_{\mathrm{F}}\left(4S_2^2\varepsilon^2 - S_0S_3\right)\right]/D_2, \tag{31b}$$

$$\alpha_{12} = \varepsilon\left(1 + \hbar^2\omega_{\mathrm{a}}\omega_{\mathrm{F}}S_2/D_2\right), \tag{31c}$$

where

$$D_2 = 1 - M_{\mathrm{F}}S_0 - MS_3 - MM_{\mathrm{F}}\left(4S_2^2\varepsilon^2 - S_0S_3\right), \tag{32a}$$

$$S_0 = \sum_{\boldsymbol{k}}\frac{d_4(\boldsymbol{k})}{d(\boldsymbol{k})}, \quad S_2 = \sum_{\boldsymbol{k}}\frac{d_3(\boldsymbol{k})}{d(\boldsymbol{k})}, \quad S_3 = \sum_{\boldsymbol{k}}\frac{\hbar\omega_{1\mathrm{F}}(\boldsymbol{k})d_3(\boldsymbol{k})}{d(\boldsymbol{k})}, \tag{32b}$$

with

$$\begin{aligned} d_3(\boldsymbol{k}) &= \hbar^3\omega_{1\mathrm{c}}^3 + \hbar^2\omega_{1\mathrm{c}}^2\left\{2J_{\mathrm{e}} + J_{\mathrm{h}}\left[\cos(k_1a) + \cos(k_2a)\right]\right\} \\ &- 2\hbar\omega_{1\mathrm{c}}J_{\mathrm{h}}^2\left[1 - \cos(k_1a)\cos(k_2a)\right] - 2J_{\mathrm{e}}J_{\mathrm{h}}^2\left[\cos(k_1a) - \cos(k_2a)\right]^2, \end{aligned} \tag{33a}$$

$$d_4(\boldsymbol{k}) = \hbar^4\omega_{1\mathrm{c}}^4 - 4\hbar^2\omega_{1\mathrm{c}}^2\left\{J_\mathrm{e}^2 + J_\mathrm{h}^2 + J_\mathrm{e}J_\mathrm{h}\left[\cos(k_1a) + \cos(k_2a)\right]\right\} + 4J_\mathrm{e}^2J_\mathrm{h}^2\left[\cos(k_1a) - \cos(k_2a)\right]^2, \tag{33b}$$

$$d(\boldsymbol{k}) = \hbar\omega_{1\mathrm{F}}(\boldsymbol{k})d_4(\boldsymbol{k}) - 4\varepsilon^2 d_3(\boldsymbol{k}). \tag{33c}$$

In case (b), 'phonon on acceptors,' expressions (31) are simpler (we recall that in that case $\xi_\mathrm{F} = 0$), notably

$$\begin{aligned} \alpha_{11} &= \hbar\omega - E_\mathrm{F} - 4W, \qquad \alpha_{12} = \varepsilon, \\ \alpha_{22} &= \hbar\omega - E_\mathrm{c} - 2J - \hbar^2\omega_\mathrm{a}^2 S_3/\left(1 - MS_3\right). \end{aligned} \tag{34}$$

3 Linear Optical Susceptibility Inside the Plane of the Quadratic Lattice

The linear optical susceptibility is isotropic inside the quadratic lattice plane and subsequently $\chi_{xx} = \chi_{yy}$. The calculations of $\chi_{xx} = \chi_{yy}$ components follow the 2D lattice models with (xy) spins. Let the x-axis is directed along the transition dipole moment of CTE_1, $\boldsymbol{p}_1$, and the y-axis along the $\boldsymbol{p}_2$ (see Figure 1). Frenkel excitons are two-fold degenerate and the operators of the transition dipole moments can read [21]

$$\hat{P} = h\left[\left(V_{x,\boldsymbol{k}=0}^+ + V_{x,\boldsymbol{k}=0}\right)\hat{x} + \left(V_{y,\boldsymbol{k}=0}^+ + V_{y,\boldsymbol{k}=0}\right)\hat{y}\right] + q\left[\left(U_{1,\boldsymbol{k}=0} - U_{3,\boldsymbol{k}=0}\right)\hat{x} + \left(U_{2,\boldsymbol{k}=0} - U_{4,\boldsymbol{k}=0}\right)\hat{y} + \mathrm{h.c.}\right], \tag{35}$$

where $V_{x,\boldsymbol{k}=0}$ and $V_{y,\boldsymbol{k}=0}$ are the annihilation operators of Frenkel excitons polarized along x- and y-axes, and h and q are the parallel to the layer components of the transition dipole moments of FEs and CTEs, respectively. The analysis of FE–CTEs coupling performed in [21] gives the following analog of the operator (5):

$$\hat{H}_{\mathrm{FE\text{–}CTEs}} = \varepsilon_1\sum_{\boldsymbol{k}}[(U_{1,\boldsymbol{k}}^+ - U_{3,\boldsymbol{k}}^+)V_{x,\boldsymbol{k}} + (U_{2,\boldsymbol{k}}^+ - U_{4,\boldsymbol{k}}^+)V_{y,\boldsymbol{k}} + \mathrm{h.c.}]. \tag{36}$$

In calculating the χ_{xx} component we need the Green functions with operators

$$V_{x,\boldsymbol{k}=0}^+(0) \quad \text{and} \quad \left[U_{1,\boldsymbol{k}=0}^+(0) - U_{3,\boldsymbol{k}=0}^+(0)\right].$$

For FEs with transition dipole moment along the x/y-axis, in the approximation of the nearest dipoles, we find the following dispersion formulas:

$$E_{\mathrm{F},x} = E_{\mathrm{F},y} = E_\mathrm{F} - V_2\left[\cos(k_1a) + \cos(k_2a)\right], \tag{37}$$

where

$$V_2 = h^2/\left(4\pi\varepsilon_0 a^3\right). \tag{38}$$

Here $\varepsilon_0 = 8.8542 \times 10^{-12}\ \mathrm{F\,m^{-1}}$ is the permittivity of free space.

When CTEs are coupled with FEs through (36) and their transition dipole moments are given by (35), the following relations hold [21]:

$$g_3^{(0)} = -g_1^{(0)}, \qquad g_2^{(0)} = -g_4^{(0)}. \tag{39}$$

It is easy to find out an analog of formula (21) for the χ_{xx} component, namely

$$\chi_{xx} = \chi_{yy} = -\frac{h^2\alpha_{22} + 4hq\alpha_{12} + 2q^2\alpha_{11}}{v\left(\alpha_{11}\alpha_{22} - 2\alpha_{12}^2\right)}, \tag{40}$$

where, for a pure excitonic region, we have

$$\alpha_{11} = \hbar(\omega - \omega_{0\mathrm{F}}) - E_\mathrm{F} + 2V_2, \quad \alpha_{12} = \varepsilon_1, \quad \alpha_{22} = \hbar(\omega - \omega_{0\mathrm{c}}) - E_\mathrm{c}, \tag{41}$$

and near the frequencies of the first vibronic replica we rederive formula (40) with the following expressions in it:

$$\alpha_{11} = \hbar\omega - E_\mathrm{F} + 2V_2 - \hbar^2\omega_\mathrm{F}^2\left[T_0 + M\left(2T_2^2\varepsilon_1^2 - T_0T_3\right)\right]/D_5, \tag{42a}$$

$$\alpha_{22} = \hbar\omega - E_\mathrm{c} - \hbar^2\omega_\mathrm{a}^2\left[T_3 + M_\mathrm{F}\left(2T_2^2\varepsilon_1^2 - T_0T_3\right)\right]/D_5, \tag{42b}$$

$$\alpha_{12} = \varepsilon_1\left(1 + \hbar^2\omega_\mathrm{a}\omega_\mathrm{F}T_2/D_5\right), \tag{42c}$$

$$D_5 = 1 - M_\mathrm{F}T_0 - MT_3 - MM_\mathrm{F}\left(2T_2^2\varepsilon_1^2 - T_0T_3\right), \tag{42d}$$

$$T_0 = \sum_{\boldsymbol{k}}\frac{\mu(\boldsymbol{k})}{D(\boldsymbol{k})}, \quad T_2 = \sum_{\boldsymbol{k}}\frac{\gamma(\boldsymbol{k})}{D(\boldsymbol{k})}, \quad T_3 = \sum_{\boldsymbol{k}}\frac{\hbar\omega_{1x}\gamma(\boldsymbol{k})}{D(\boldsymbol{k})}, \tag{42e}$$

where

$$\mu(\boldsymbol{k}) = \hbar\omega_{1y}d_4(\boldsymbol{k}) - 2\varepsilon_1^2\hbar\omega_{1\mathrm{c}}\left\{D_6 - J_\mathrm{h}^2\left[\sin(k_1a) + \sin(k_2a)\right]^2\right\}, \tag{43a}$$

$$\gamma(\boldsymbol{k}) = \hbar^2\omega_{1y}\omega_{1\mathrm{c}}\left\{D_6 - J_\mathrm{h}^2\left[\sin(k_1a) - \sin(k_2a)\right]^2\right\} - 2\varepsilon_1^2D_6, \tag{43b}$$

with

$$D(\boldsymbol{k}) = \hbar\omega_{1x}\mu(\boldsymbol{k}) - 2\varepsilon_1^2\gamma(\boldsymbol{k}), \tag{44}$$

$$D_6 = \hbar^2\omega_{1\mathrm{c}}^2 - \left\{2J_\mathrm{e} + J_\mathrm{h}\left[\cos(k_1a) + \cos(k_2a)\right]\right\}^2, \tag{45}$$

and

$$\hbar\omega_{1x} = \hbar\omega_{1y} = \hbar\left(\omega - \omega_0 - \Omega_{1\mathrm{F}}\right) - E_{\mathrm{F},x,y}. \tag{46}$$

4 Numerical Simulations of the Excitonic and Vibronic Spectra

In this section, we calculate the excitonic density of states (DOSs) and the linear absorption spectra as imaginary parts of (21) and (40) in which we take $\hbar\omega + \mathrm{i}\delta$

instead of $\hbar\omega$. The small imaginary addend, $\delta = 1 \times 10^{-3}$ eV (in calculating of a DOS, $\delta = 1 \times 10^{-4}$ eV), expresses the final width of the excitonic lines. Our parametrization is based on the typical values of the excitonic and vibrational parameters but it is not closely related to fixed molecules and crystals.

We use three set of parameters:

(A) a set similar to that of the anthracene-PMDA crystal [12], namely:
$E_{\mathrm{F}} = 2.355$ eV, $E_{\mathrm{c}} = 2.31$ eV, $\hbar\omega_1 = 0.079$ eV,
$\xi = 0.7$, $\xi_{\mathrm{F}} = 0.9$, $\varepsilon = 0.02$ eV,
$|J_{\mathrm{e}}| = |J_{\mathrm{h}}| = 0.002$ eV, $W = V_2 = 0.005$ eV.

In calculating Im χ_{zz}, we put $|p_{\mathrm{F}z}| = 10|p_{\mathrm{c}z}|$, whereas in calculating Im χ_{xx} we take $h = 2q$ (see (40)).

The other networks of parameters are close to the excitonic and vibrational parameters of the PTCDA and MePTCDI crystals (see, e.g., [22]). Those crystals do not exhibit square symmetry and our calculations do not simulate their spectra. We use the following sets of data:

(B) $E_{\mathrm{F}} = 2.34$ eV, $E_{\mathrm{c}} = 2.27$ eV, $\hbar\omega_0 = 0.17$ eV,
$\xi_{\mathrm{F}} = 0.9$, $\varepsilon = 0.02$ eV,
$W = V_2 = 0.01$ eV, $|J_{\mathrm{e}}| = |J_{\mathrm{h}}| = 0.003$ eV.

(C) $E_{\mathrm{F}} = 2.23$ eV, $E_{\mathrm{c}} = 2.15$ eV, $\hbar\omega_0 = 0.17$ eV,
$W = V_2 = 0.005$ eV,
$|J_{\mathrm{e}}| = |J_{\mathrm{h}}| = 0.003/0.004$ eV, $\varepsilon = \pm 0.02$ eV.

Figure 2 illustrates the renormalization of the excitonic DOS caused by the FE–CTEs coupling. The DOS's calculations are based on the corresponding dispersion formulas by using the expressions [15, 16]

$$\rho_z = -2\pi \mathrm{Im}\, S_0, \quad \rho_x = -\pi \mathrm{Im}\, T_0 \ \text{ at } \ \omega_0 = \xi = \xi_{\mathrm{F}} = 0 \ \text{ and } \ \delta \to +0. \qquad (47)$$

Excitonic DOS manifests 2D behavior [23] with non-zero values at the boundaries of the excitonic bands and logarithmic singularities inside the bands which correspond to the saddle points in dispersion curves (4) and (37). FE–CTEs coupling causes a splitting of the excitonic bands near the E_{F} and E_{c} levels, as well as the appearance of two logarithmic spikes near the energy level of 2.37 eV. Near the region of 2.30–2.32 eV, two weak bands split from the lower excitonic band (the CTEs' band).

The linear absorption spectra of pure FEs ($\varepsilon = 0$) calculated using (21) and (31) for Im χ_{zz} and (40)–(42) for Im χ_{xx} are shown in Figure 3. The excitonic spectra near 2.30 eV as well as the first vibronics near 2.37 eV, the second vibronics near 2.45 eV, and even the third vibronics near 2.53 eV, separated by an energetic distance equal approximately to $\hbar\omega_1 \approx 0.08$ eV, split for both polarizations: perpendicular to the 2D plane (red curve) and inside the plane (green curve). The excitonic lines and the absorption near the first vibronics exhibit a Lorentz-type

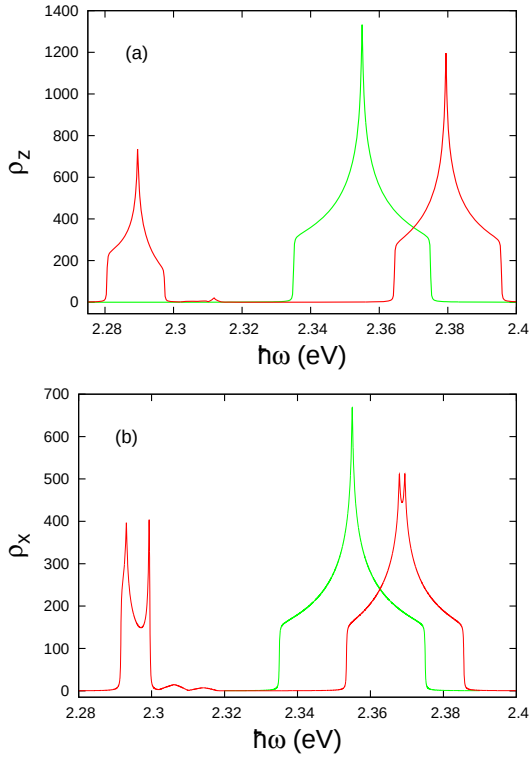

Figure 2. Excitonic density of states. Panel (a): ρ_z computed from (4). Panel (b): ρ_x computed from (37). Green curves: DOS of pure FEs ($\varepsilon = 0$); red curves: renormalized DOS as a result of FE–CTEs coupling ($E_{\mathrm{F}} = 2.355$ eV, $E_{\mathrm{c}} = 2.31$ eV, $W = V_2 = 0.005$ eV, $J_{\mathrm{e}} = J_{\mathrm{h}} = 0.002$ eV, $\varepsilon = 0.02$ eV).

lineshape which corresponds to one-particle (bound) FE–phonon states. But FE–phonon coupling cannot bind the FE and phonons near 2.45 eV and 2.53 eV, and the calculated absorption spectra represent continua of many-particle (MP) states.

The absorption spectra of pure CTEs ($\varepsilon = 0$) near the excitonic line of 2.27 eV and first two vibronics can be seen in Figure 4 (see also [15]). The sign of the transfer integrals J_{e}, J_{h} influences the absorption with z-polarization (red and green curves) and it has no impact on the absorption with x-polarization. The lineshape of the vibronic lines near 2.35 eV is lightly wider than the excitonic lines near 2.27 eV, but the second vibronic spectra near 2.43 eV demonstrate the behavior of MP continua.

Figure 5 illustrates the case of FE–CTEs coupling with excitonic parameters used in Figures 3 and 4. The linear absorption spectra of the z-polarization pos-

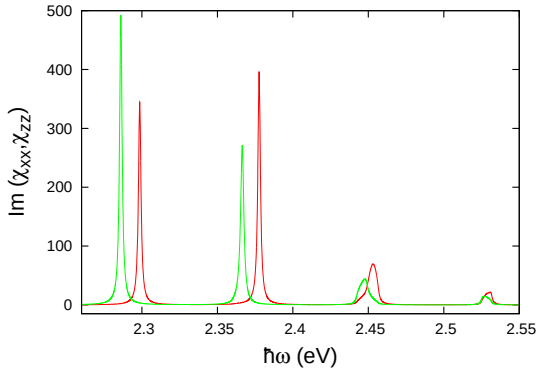

Figure 3. Linear absorption spectra of pure FEs ($\varepsilon = 0$) with $E_{\mathrm{F}} = 2.355$ eV, $W = 0.005$ eV, $\hbar\omega_0 = 0.079$ eV, $\xi_{\mathrm{F}} = 0.9$. Red curve: Im χ_{zz}; green curve: Im χ_{xx}.

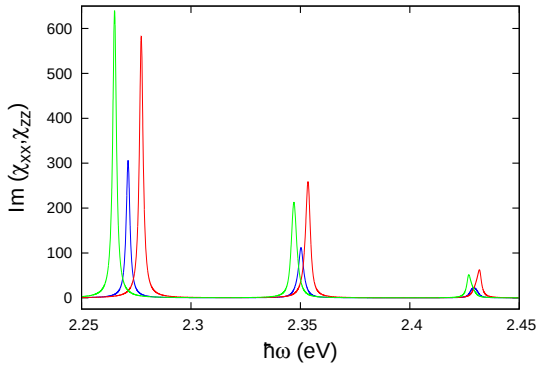

Figure 4. Linear absorption spectra of pure CTEs ($\varepsilon = 0$) with $E_{\mathrm{c}} = 2.31$ eV, $\hbar\omega_0 = 0.079$ eV, $\xi = 0.7$ ($\xi_{\mathrm{F}} = 0$). Blue curve: Im χ_{xx} ($J_{\mathrm{e}} = J_{\mathrm{h}} = 0.002$ eV); red curve: Im χ_{zz} ($J_{\mathrm{e}} = J_{\mathrm{h}} = 0.002$ eV); green curve: Im χ_{zz} ($J_{\mathrm{e}} = J_{\mathrm{h}} = -0.002$ eV).

sess two components that correspond to the renormalized CTEs (the lower component) and to FEs (the upper one). A splitting of the spectra of xy-polarizations (green curve) is practically absent. Comparing the spectra of Figures 3–5 we observe the strong impact of the FE–CTEs coupling in the excitonic region (2.25–2.32 eV), in the first vibronic spectra (2.33–2.39 eV), in the second vibronics (2.42–2.46 eV), etc. The lineshape of the excitonic and first vibronic maxima is Lorentzian, whereas the second and third vibronic lines represent the continua of the MP states.

Figure 6 and the following figures show the absorption in the 'phonon on donors' case ($\xi \neq 0$, $\xi_{\mathrm{F}} \neq 0$). If the CTEs–phonon coupling is relatively weak (see Figure 6), the FE–CTEs coupling causes a two-fold splitting in the excitonic

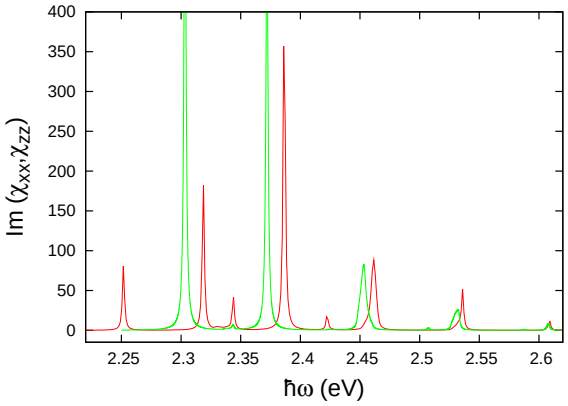

Figure 5. Excitonic and vibronic spectra in the case of FE–CTEs coupling with $E_{\mathrm{F}} = 2.355$ eV, $E_{\mathrm{c}} = 2.31$ eV, $\hbar\omega_0 = 0.079$ eV, $W = V_2 = 0.005$ eV, $J_{\mathrm{e}} = J_{\mathrm{h}} = 0.002$ eV, $\varepsilon = 0.02$ eV, $\xi_{\mathrm{F}} = 0.9$, $\xi = 0.7$; red curve: $\operatorname{Im}\chi_{zz}$ ($p_{\mathrm{F}z} = 10p_{\mathrm{c}z}$); green curve: $\operatorname{Im}\chi_{xx}$ ($h = 2q$). Excitonic region: 2.25–2.32 eV; first vibronic region: 2.33–2.39 eV; second vibronics: 2.42–2.46 eV, etc.

spectra with z-polarization, notably intensive maxima of FEs near 2.22 eV, and weak maxima near 2.17–2.18 eV (only one strong maximum of x-polarization near 2.21 eV appears).

The absorption curves in Figure 7 have been calculated by using vibronic for-

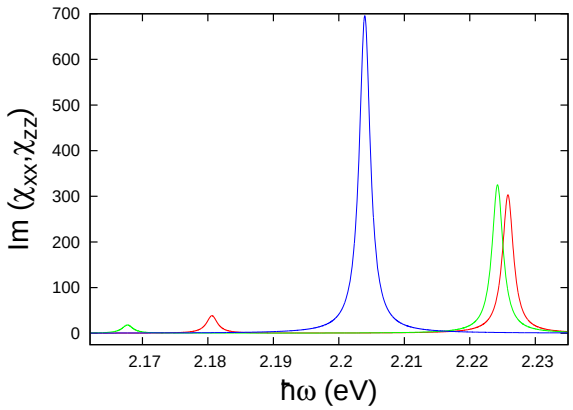

Figure 6. Linear absorption spectra in the excitonic region for the 'phonon on donors' case: $E_{\mathrm{F}} = 2.34$ eV, $E_{\mathrm{c}} = 2.27$ eV, $\hbar\omega_0 = 0.17$ eV, $\xi = 0.5$, $W = V_2 = 0.01$ eV, $J_{\mathrm{e}} = J_{\mathrm{h}} = 0.003$ eV, $\varepsilon = 0.02$ eV, $\xi_{\mathrm{F}} = 0.9$. $\operatorname{Im}\chi_{zz}$: red curve with $J_{\mathrm{e}} = J_{\mathrm{h}} = 0.003$ eV, green curve with $J_{\mathrm{e}} = J_{\mathrm{h}} = -0.003$ eV. $\operatorname{Im}\chi_{xx}$: blue curve. The calculations are based on (21) and (40) together with (22) and (41).

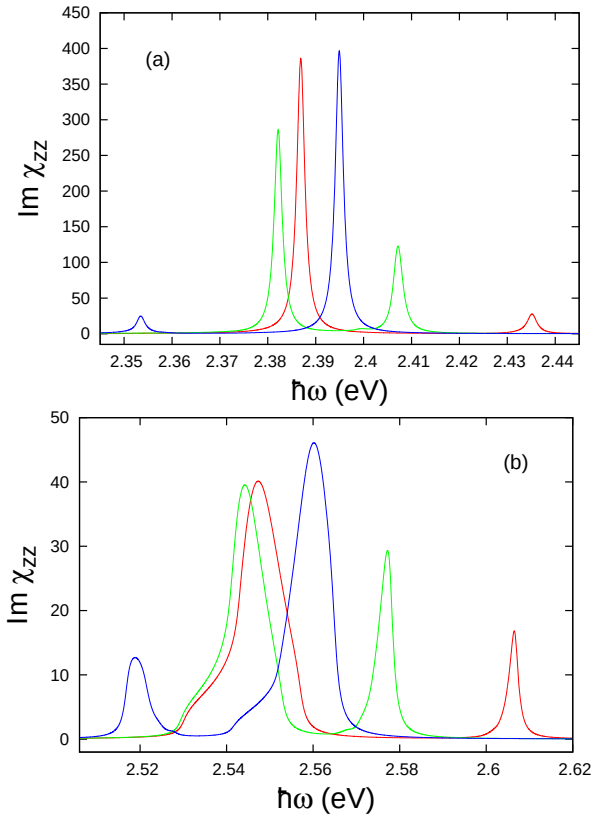

Figure 7. Linear absorption spectra in the vibronic region, z-polarization (see the parameters of Figure 6). The different absorption curves correspond to the following values of the CTEs–phonon coupling parameter: green curve $\xi = 0.5$, blue curve $\xi = 0.7$, and red curve $\xi = 1.025$. Panel (a): One-phonon vibronic spectra. Panel (b): Two-phonon vibronic spectra.

mulas (31). The one-phonon vibronic spectra, Figure 7(a), are dominated by one-particle maxima near 2.38–2.41 eV and the FEs–CTEs splitting is manifested most strongly in the case of $\xi = 0.5$ (green curve). Two-phonon vibronic spectra shown in Figure 7(b) consist of wide and not very intensive continua of MP states. We note the splitting of all absorption two-phonon curves – each one contains two continua corresponding to FEs and CTEs.

The linear absorption in the case of relatively weak FE–phonon and CTEs–phonon couplings has been calculated using formulas (31) and (42) at $\xi_{\mathrm{F}} = 0.6$, $\xi = 0.4$ (Figure 8). The most intensive absorption can be expected in the excitonic spectra and partly in one-phonon vibronic spectra. Because of relatively weak exciton–phonon coupling the vibronic spectra consist of not inten-

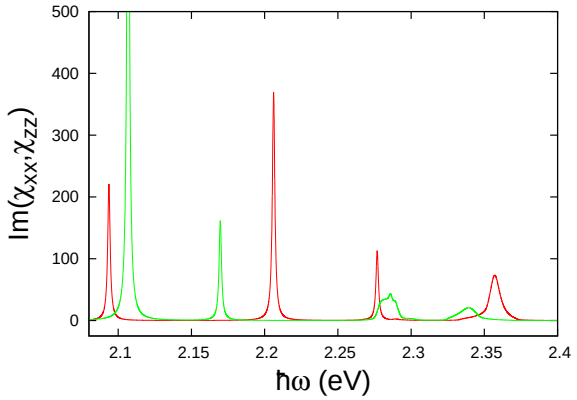

Figure 8. Linear absorption in the excitonic and vibronic regions: $E_{\mathrm{F}} = 2.23$ eV, $V, E_{\mathrm{c}} = 2.15$ eV, $\hbar\omega_0 = 0.17$ eV, $W = V_2 = 0.01$ eV, $J_{\mathrm{e}} = J_{\mathrm{h}} = -0.004$ eV, $\varepsilon = -0.02$ eV, $\xi_{\mathrm{F}} = 0.6$, $\xi = 0.4$. Im χ_{zz}: red curve, Im χ_{xx}: green curve. The excitonic region is 2.1–2.2 eV and the one-phonon vibronic spectra occupy the region of 2.27–2.36 eV.

sive continua of MP exciton–phonon states. In this case, the manifestation of two-phonon vibronic spectra would be very difficult in real experiments. In the excitonic spectra the two-fold splitting caused by the FEs–CTEs coupling is well expressed.

The opposite case of relatively strong exciton–phonon coupling is illustrated in Figure 9. The excitonic spectra are located below 2.1 eV, one-phonon vi-

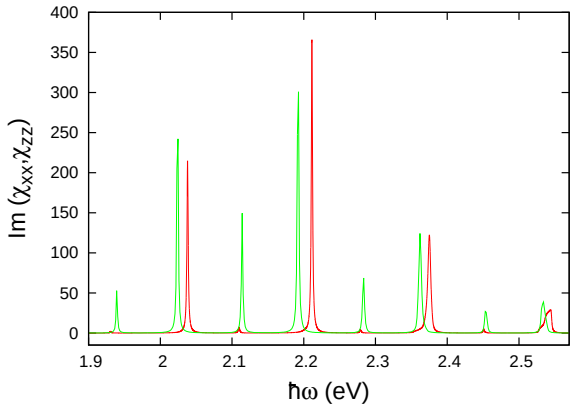

Figure 9. Linear absorption with strong exciton–phonon coupling ($\xi = \xi_{\mathrm{F}} = 1.1$) with $E_{\mathrm{F}} = 2.23$ eV, $E_{\mathrm{c}} = 2.15$ eV, $\hbar\omega_0 = 0.17$ eV, $W = V_2 = 0.005$ eV, $\varepsilon = 0.02$ eV, $J_{\mathrm{e}} = J_{\mathrm{h}} = -0.003$ eV. Red curve: Im χ_{zz}; green curve: Im χ_{xx}.

bronic spectra are displayed in the region 2.11–2.21 eV, while two-phonon vibronic spectra are located in the 2.28–2.39 eV's region, and so on. We note here that the E_{F} value of the FE's level and the E_{c} value of CTEs can be shifted in the calculations intending to obtain the coincidence between calculated and observed excitonic lines (see [18]). Due to the strong coupling, the intensities of the linear absorption in the excitonic and one/two-phonon vibronic lines are comparable and they correspond to one-particle exciton–phonon states. The two 'components' of the green curve which are genetically associated with CTEs and FEs, respectively, can be distinguished whereas the linear absorption of the z-polarizations exhibits one component only (the lower one is very weak).

Our simulations of the linear absorption spectra show the different impacts of the FE–CTEs coupling depending on the exciton–phonon coupling. In the case of weak values of ξ and ξ_{F} parameters, the two-fold splitting manifests itself in the z-polarization, whereas by increasing the values of ξ and ξ_{F} we obtain the spectra's splitting of the xy-polarization.

Part B: Excitons in a Hexagonal Graphene-Like Donor–Acceptor Lattice

We use geometry of two hexagonal sublattices in graphene, but instead of two identical entities (in graphene two carbon atoms) in the donor–acceptor 2D system the one sublattice determines the positions of donors and the other sublattice fixes the posotions of acceptors (see Figure 10). The positions of donors define the nodes of the 2D lattice, and consequently, the holes in CTEs. The nearest DA

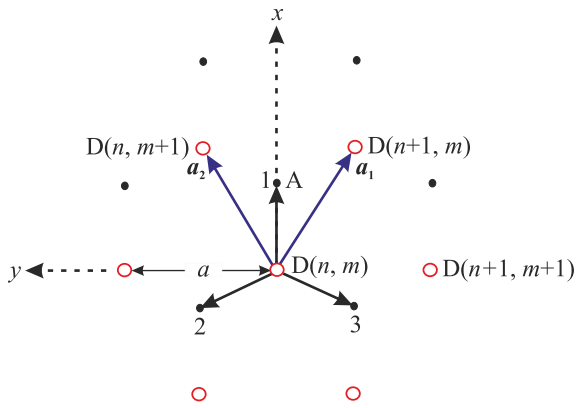

Figure 10. Two hexagonal sublattices of donors (white circles) and acceptor (black dots). $\boldsymbol{a}_1$ and $\boldsymbol{a}_2$ are the lattice vectors; numerals 1–3 denote three identical CTEs; (xy) is a orthogonal coordinate system, and a is the lattice constant.

pairs govern the trigonal symmetry of the identical CTEs (in the case of a $120°$-rotation around the hexagonal axis). The calculations are performed in a orthogonal system (x, y, z) in which the x-axis is directed along the transition dipole component $\boldsymbol{p}_1$ (0bviously the moduli of $\boldsymbol{p}_1$, $\boldsymbol{p}_2$, and $\boldsymbol{p}_3$ are equal; the same is valid for the perpendicular to the lattice plane components $p_{1z} = p_{2z} = p_{3z}$, that are very small, see Part A; z-axis being perpendicular to the layer).

5 Collectivization of CTEs and Frenkel Excitons

By using the trigonal symmetry of CTEs and exploring the identical quasiparticles in a way described in the Appendix of Ref. [21], we find the following linear combinations of CTEs wave functions $C_i^+|0\rangle$, where $i = 1, 2, 3$ (we do not write the node of the donor of a CTE):

$$\Psi_{\rm c}|0\rangle = \left[a_1 C_1^+ + a_2 C_2^+ + a_2 C_2^+\right]|0\rangle, \tag{48}$$

where

$$a_1 = 1/\sqrt{3}, \quad a_2 = a_1 \exp(\mathrm{i}\beta), \quad \text{and} \quad a_2 = a_1 \exp(2\mathrm{i}\beta) \tag{49}$$

with βs being the roots of the equation

$$\exp(3\mathrm{i}\beta) = 1. \tag{50}$$

Obviously $\beta = 2\pi/3$, $4\pi/3$, and 2π, leading to the following linear combinations:

$$\Psi_1|0\rangle = \frac{1}{\sqrt{3}}\Big[C_1^+ - \frac{1}{2}(C_2^+ + C_3^+) + \mathrm{i}\frac{\sqrt{3}}{2}(C_2^+ - C_3^+)\Big]|0\rangle \ \text{ for } \ \beta = \frac{2}{3}\pi, \tag{51}$$

$$\Psi_2|0\rangle = \frac{1}{\sqrt{3}}\Big[C_1^+ - \frac{1}{2}(C_2^+ + C_3^+) - \mathrm{i}\frac{\sqrt{3}}{2}(C_2^+ - C_3^+)\Big]|0\rangle \ \text{ for } \ \beta = \frac{4}{3}\pi, \tag{52}$$

$$\Psi_3|0\rangle = \frac{1}{\sqrt{3}}(C_1^+ + C_2^+ + C_3^+)|0\rangle \qquad \text{for } \ \beta = 2\pi. \tag{53}$$

The most intensive transfers of CTEs are caused by transitions of the electron of a CTE (or of its hole) on the nearest acceptors (donors). In this way, we find the following CTEs part of the Hamiltonian (see also [15]):

$$\begin{aligned}\hat{H}_{\rm CTEs} = \sum_{nm,\, i=1\text{–}3} \Big[& E_{\rm c} C_{i,nm}^+ C_{i,nm} \\ & + J_{\rm e}(C_{2,nm}^+ C_{1,nm} + C_{3,nm}^+ C_{2,nm} + C_{1,nm}^+ C_{3,nm} + \text{h.c.}) \\ & + J_{\rm h}(C_{2,n+1\,m}^+ C_{1,nm} + C_{3,n-1\,m+1}^+ C_{2,nm} + C_{1,n\,m-1}^+ C_{3,nm} + \text{h.c.})\Big],\end{aligned} \tag{54}$$

where $E_{\rm c}$ is the excitation energy of CTEs, and $J_{\rm e}$, $J_{\rm h}$ are the transfer integrals of the electron and hole, respectively.

By using the Fourier components of the CTEs operators in the momentum space $\boldsymbol{k} = (k_1, k_2)$, we obtain the following analog of expression (2):

$$\hat{H}_{\rm CTEs} = \sum_{\boldsymbol{k},\, i=1\text{–}3} \big[E_{\rm c} C_{i\boldsymbol{k}}^{+} C_{i\boldsymbol{k}} + C_{3\boldsymbol{k}}^{+} C_{2\boldsymbol{k}} + C_{1\boldsymbol{k}}^{+} C_{3\boldsymbol{k}} + {\rm h.c.}\big) + J_{\rm h}\left(C_{2\boldsymbol{k}}^{+} C_{1\boldsymbol{k}} \exp(-{\rm i}k_1\gamma) + C_{3\boldsymbol{k}}^{+} C_{2\boldsymbol{k}} \exp[{\rm i}(k_1 - k_2)\gamma] + C_{1\boldsymbol{k}}^{+} C_{3\boldsymbol{k}} \exp({\rm i}k_2\gamma) + {\rm h.c.}\right)\big]. \quad (55)$$

Here, $\gamma = \sqrt{3}a/2$, where, recall, a is the lattice constant.

As in Part A, Frenkel excitons come from the electronic excitations of donors. Their collectivization, influenced by the hexagonal symmetry and studied in Ref. [16], causes the appearance of two types of excitons:

(a) Non-degenerate FEs. Dipole active FEs of this type have transition dipole moment, $p_{{\rm F}z}$, perpendicular to the layer, and their contribution to the Hamiltonian is:

$$\hat{H}_{\rm FE}^{(z)} = \sum_{k} \left(E_{\rm F} + 2W\mu\right) B_{z,k}^{+} B_{z,k} \quad (56)$$

with $\mu = \cos(k_1\gamma) + \cos(k_2\gamma) + \cos[(k_1 - k_2)\gamma]$. Here, $E_{\rm F}$ is the excitation energy of FEs, and W is their transfer integral between the neighbor donors.

(b) Degenerate FEs with transition dipole moments parallel to the layer. Due to isotropy in the 2D lattice plane, the components of those moments on x and y axes are equal. We denote by $B_{x,k}$ and $B_{y,k}$ the operators of annihilation of FEs with transition dipole moments along x and y axes and obtain the following combinations (see [16]):

$$\Psi_{{\rm FE},1}|0\rangle = \frac{1}{\sqrt{2}}\left(B_x^{+} + {\rm i}B_y^{+}\right)|0\rangle \quad \text{for} \quad \beta = 2\pi/3, \quad (57a)$$

$$\Psi_{{\rm FE},2}|0\rangle = \frac{1}{\sqrt{2}}\left(B_x^{+} - {\rm i}B_y^{+}\right)|0\rangle \quad \text{for} \quad \beta = 4\pi/3, \quad (57b)$$

We obtain the following contributions to the Hamiltonian:

$$\hat{H}_{\rm FE}^{(x,y)} = \sum_{k} [E_{{\rm F},1}(B_{x,k}^{+} B_{x,k} + B_{y,k}^{+} B_{y,k}) + W_x B_{x,k}^{+} B_{x,k} + W_y B_{y,k}^{+} B_{y,k}], \quad (58)$$

where $E_{{\rm F},1}$ is the excitation energy of degenerate FEs,

$$W_x = 2V_1 \left\{-\frac{5}{4}\left[\cos(k_1\gamma) + \cos(k_2\gamma)\right] + \cos[(k_1 - k_2)\gamma]\right\}, \quad (59)$$

and

$$W_y = 2V_1 \left\{\frac{1}{4}\left[\cos(k_1\gamma) + \cos(k_2\gamma)\right] - 2\cos[(k_1 - k_2)\gamma]\right\}. \quad (60)$$

Above expressions (59) and (60) have been calculated using the transition dipole–dipole nearest neighbor approximation, notably

$$V_1 = \frac{h^2}{4\pi\varepsilon_0 a^3}, \tag{61}$$

where h is the transition dipole moment of degenerate FEs.

The coupling of FEs and CTEs can be implemented through the transition of an electron from a neutral exited molecule (with a FE on it) to one of neighbor acceptors (see [12]). The nonvanishing coupling terms must be transformed in the case of rotation around the hexagonal axis via multiplication by the same factor $\exp(\mathrm{i}\beta)$. In this way, we find the following coupling parts of the Hamiltonian:

(i) for non-degenerate FEs with transition dipole moment along z-axis:

$$\hat{H}^{(z)}_{\mathrm{FCTE}} = \sum_{k,\, i=1,2,3} \left(C^{+}_{i,k} B_{z,k} + \mathrm{h.c.} \right). \tag{62}$$

The transition dipole moment can be presented in the form:

$$\hat{P}_z = p_{\mathrm{F}z} \left(B_{z,k=0} + \mathrm{h.c.} \right) + p_z \sum_{i=1,2,3} \left(C_{i,k=0} + \mathrm{h.c.}. \right) \tag{63}$$

(ii) For degenerate FEs with transition dipole moments parallel to the layer we have

$$\begin{aligned} \hat{H}^{(x,y)}_{\mathrm{FCTE}} \; &= \varepsilon_1 \sum_k \Big\{ \Big[C^{+}_{1,k} - \frac{1}{2}(C^{+}_{2,k} + C^{+}_{3,k}) \\ &\quad + \mathrm{i}\frac{\sqrt{3}}{2}(C^{+}_{2,k} - C^{+}_{3,k}) \Big] (B_x - \mathrm{i}B_y) + \mathrm{h.c.} \Big\} \\ &\quad + \varepsilon_2 \sum_k \Big\{ \Big[C^{+}_{1,k} - \frac{1}{2}(C^{+}_{2,k} + C^{+}_{3,k}) \\ &\quad - \mathrm{i}\frac{\sqrt{3}}{2}(C^{+}_{2,k} - C^{+}_{3,k}) \Big] (B_x + \mathrm{i}B_y) + \mathrm{h.c.} \Big\} \end{aligned} \tag{64}$$

Owing to the isotropy of the linear optical susceptibility, $\chi_{xx} = \chi_{yy}$, in the lattice plain and using a proper choice of the phases of wave functions $B^{+}_{x}|0\rangle$ and $C^{+}_{1}|0\rangle$, we can obtain the identity of the coupling parameters

$$\varepsilon_1 = \varepsilon_2 = \varepsilon_{\mathrm{a}}/2. \tag{65}$$

Then the coupling part of the Hamiltonian reduces to

$$\begin{aligned} \hat{H}^{(x,y)}_{\mathrm{FCTE}} = \varepsilon_{\mathrm{a}} \sum_k \Big\{ \Big[C^{+}_{1,k} - \frac{1}{2}(C^{+}_{2,k} + C^{+}_{3,k}) \Big] B_{x,k} \\ + \frac{\sqrt{3}}{2}(C^{+}_{2,k} - C^{+}_{3,k}) B_{y,k} + \mathrm{h.c.} \Big\}. \end{aligned} \tag{66}$$

The operator of the transition dipole moment, $\hat{P}_{x,y}$, takes the form

$$\hat{P}_{x,y} = h\left(B_{x,k=0}\hat{x} + B_{y,k=0}\hat{y} + \text{h.c.}\right) + q\Big\{\Big[C_{1,k=0} - \frac{1}{2}(C_{2,k=0} + C_{3,k=0})\Big]\hat{x} + \frac{\sqrt{3}}{2}(C_{2,k=0} - C_{3,k=0})\hat{y} + \text{h.c.}\Big\}, \quad (67)$$

where q is the component of the transition dipole moment of CTEs parallel to the layer.

For describing the exciton–phonon coupling along with the way of calculating the linear optical susceptibility follow Sections 2 and 3 of Part A.

6 Excitonic and Vibronic Spectra

Here, we reproduce the final formulas only that have been obtained using, mutatis mutandis, the approach of Part A for the case of a 2D hexagonal lattice. The component χ_{zz} for the light polarized perpendicular to the layer is (see (21))

$$\chi_{zz} = -\frac{1}{v\left(\alpha_{11}\alpha_{22} - 3\alpha_{12}^2\right)}\left(p_{\mathrm{F}z}^2\alpha_{22} + 6p_{\mathrm{F}z}p_z\alpha_{12} + 3p_z^2\alpha_{11}\right), \quad (68)$$

where v is the volume occupied by one donor–acceptor pair,

$$\alpha_{11} = \hbar\left(\omega - \Omega_{0\mathrm{F}}\right) - E'_{\mathrm{F}} - 6W, \quad \alpha_{12} = \varepsilon, \qquad \alpha_{22} = \hbar\left(\omega - \Omega_{0\mathrm{c}}\right) - E_{\mathrm{c}} - 2\left(J_{\mathrm{e}} + J_{\mathrm{h}}\right). \quad (69)$$

The $\chi_{xx} = \chi_{yy}$ components for the light polarized in the plane of the hexagonal lattice are (see (40))

$$\chi_{xx} = \chi_{yy} = -\frac{h^2\alpha_{22} + 3qh\alpha_{12} + (3/2)q^2\alpha_{11}}{v(\alpha_{11}\alpha_{22} - 3\alpha_{12}^2/2)}, \quad (70)$$

where

$$\alpha_{11} = \hbar\left(\omega - \Omega_{0\mathrm{F}}\right) - E'_{\mathrm{F}} + 3V_1, \quad \alpha_{12} = \varepsilon_{\mathrm{a}}, \qquad \alpha_{22} = \hbar\left(\omega - \Omega_{0\mathrm{c}}\right) - E_{\mathrm{c}} + J_{\mathrm{e}} + J_{\mathrm{h}}. \quad (71)$$

In calculating one-phonon vibronic spectra, the χ_{zz} component is given by formula (68) and the $\chi_{xx} = \chi_{yy}$ components correspondingly by formula (70). All formulas for the functions α_{11}, α_{12}, and α_{22} in the case of one-phonon vibronic spectra have been calculated by means of methodics used in Part A.

7 Numerical Simulations of Excitonic and Vibronic Spectra

In this section, we simulate the linear absorption spectra of the hexagonal DA lattice using the methodics and three sets of parameters listed in Sect. 4, Part A.

Figure 11 illustrates the excitonic DOS of excitons with transition dipole moment perpendicular to the layer. The green curve concerns FEs only (see the calculations in [18]). The FE–CTEs coupling causes the splitting of a second band near the E_{c}-level of CTEs.

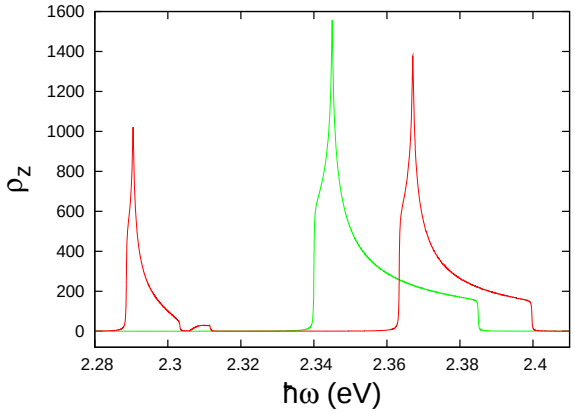

Figure 11. Excitonic DOS ρ_z of non-degenerate excitons at $E_{\mathrm{F}} = 2.355$ eV, $E_{\mathrm{c}} = 2.31$ eV, $W = 0.005$ eV. Green curve: $\varepsilon = 0$ (without FE–CTEs coupling); red curve: $\varepsilon = 0.02$ eV.

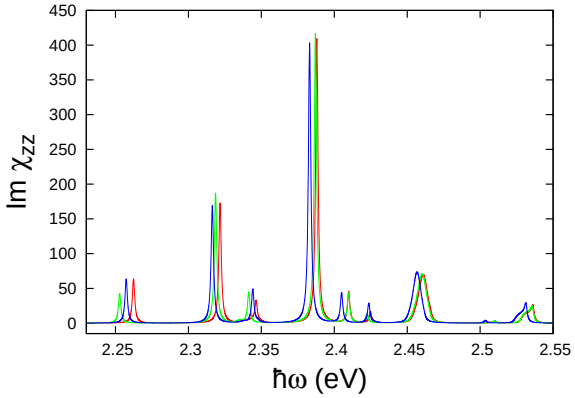

Figure 12. Linear absorption spectra of the z-polarization with $E_{\mathrm{F}} = 2.355$ eV, $E_{\mathrm{c}} = 2.31$ eV, $\hbar\omega_0 = 0.079$ eV, $\varepsilon = 0.02$ eV, $W = 0.005$ eV, $\xi_{\mathrm{F}} = 0.9$, and $\xi = 0.7$. Red curve corresponds to $J_{\mathrm{e}} = J_{\mathrm{h}} = 0.002$ eV; green curve to $J_{\mathrm{e}} = J_{\mathrm{h}} = -0.002$ eV; blue curve to $J_{\mathrm{e}} = -J_{\mathrm{h}} = 0.002$ eV).

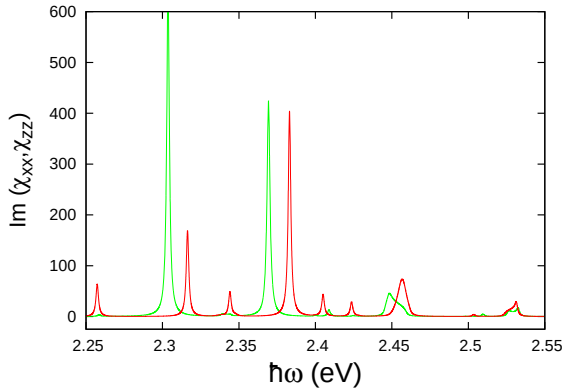

Figure 13. Linear absorption spectra of the z-polarization (red curve) and (xy)-polarization (green curve) at the same parameters as in Figure 12, but with $J_{\mathrm{e}} = -J_{\mathrm{h}} = 0.02$ eV.

The linear absorption spectra in the case"vibration on donors" are depicted in Figure 12, in which the frequencies below 2.33 eV correspond to the excitonic spectra of coupled CTEs (near 2.25 eV) and FEs (near 2.32 eV). The one-phonon vibronic spectra are situated in the frequency region of 2.33–2.42 eV, whereas the two-phonon vibronic spectra lie in the region of 2.42–2.5 eV, etc. The different signs of the J_{e} and J_{h} parameters influence primarily the CTEs lines and their first vibronic replica near 2.34 eV. We note the appearance of two vibronic maxima near 2.4 eV (the higher one is very weak). The excitonic and one-phonon vibronic spectra correspond to bound exciton–phonon states, whereas the two- and three-phonon spectra are related to the MP unbound states.

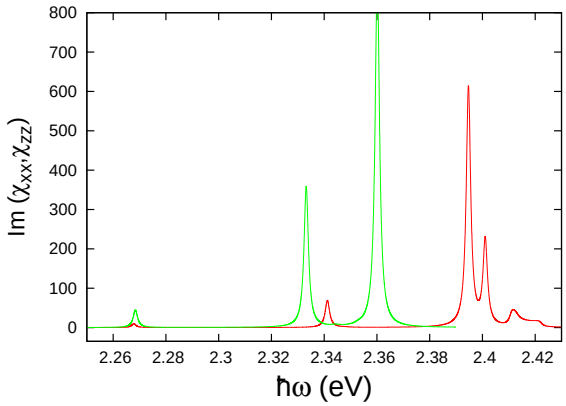

Figure 14. Linear absorption spectra in the case "phonon on acceptors" ($\xi_{\mathrm{F}} = 0$, the other parameters are the same as in Figures 12 and 13). Red curve: z-polarization, green curve: (xy)-polarization.

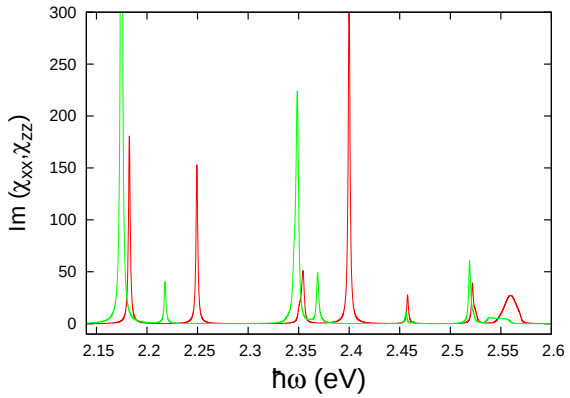

Figure 15. Linear absorption spectra of coupled excitons at $E_{\mathrm{F}} = 2.34$ eV, $E_{\mathrm{c}} = 2.27$ eV, $\hbar\omega_0 = 0.17$ eV, $W = V_1 = 0.01$ eV, $\varepsilon = -0.02$ eV, $J_{\mathrm{e}} = -J_{\mathrm{h}} = 0.004$ eV, $\xi_{\mathrm{F}} = 0.9$, $\xi = 0.7$. Red curve: Im χ_{zz}; green curve: Im χ_{xx}.

The linear absorption of the two polarizations (perpendicular to the layer – red curve – and parallel to the layer – green curve) is depicted in Figure 13.The two Lorentz-type maxima of the green curve are more significant and they correspond to a FE and its first vibronic replica. The two- and three-phonon replicas of the green and red curves lie in coinciding frequency regions and describe unbound exciton–phonon states.

Figure 14 illustrates the case where the intramolecular vibration belongs to the acceptors ($\xi_{\mathrm{F}} = 0$). As a rule, the spectra consist of a small numbers of absorp-

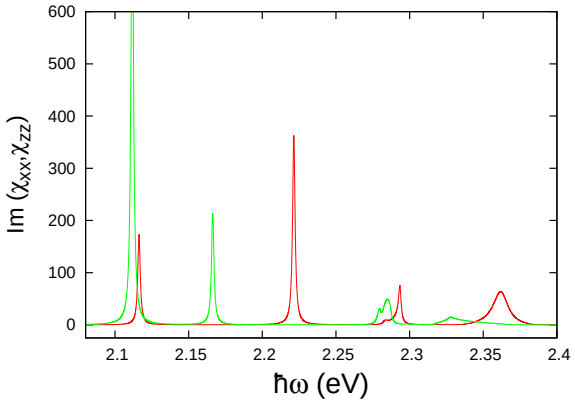

Figure 16. Linear absorption spectra in the case of weak exciton–phonon coupling at $E_{\mathrm{F}} = 2.23$ eV, $E_{\mathrm{c}} = 2.15$ eV, $\hbar\omega_0 = 0.17$ eV, $\varepsilon = -0.02$ eV, $W = V_1 = 0.01$ eV, $J_{\mathrm{e}} = -J_{\mathrm{h}} = 0.004$ eV, $\xi_{\mathrm{F}} = 0.6$, $\xi = 0.4$. Red curve: Im χ_{zz}, green curve: Im χ_{xx}.

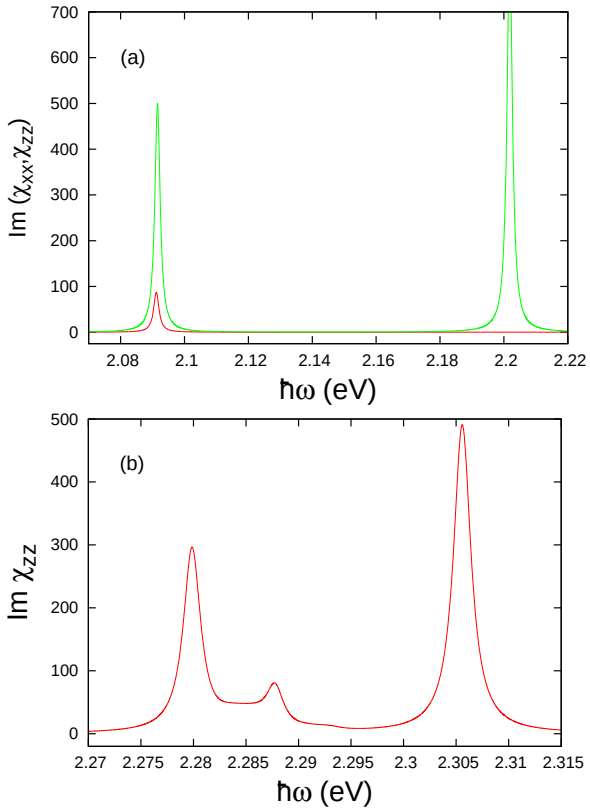

Figure 17. Linear absorption spectra in the case of "vibration on acceptors" ($\xi_{\mathrm{F}} = 0$). The values of other parameters are the same as in Figure 16. Red curves: $\mathrm{Im}\,\chi_{zz}$, green curves: $\mathrm{Im}\,\chi_{xx}$. Panel (a): Excitonic spectra using formulas (68) and (70). Panel (b): One-phonon vibronic spectrum.

tion lines, usually the lines of CTEs and their first vibronics (in Figure 14 near 2.26 eV and 2.33 eV for the green curve, and near 2.34 eV and 2.41 eV ro the red one) and the line of a FE (in Figure 14 the intensive maxima at 2.36 eV and 2.39 eV). The interpretation of the absorption lines in the case of a FE that originates from donors but the vibration belongs to acceptors (or vice versa) might be more problematic.

The linear absorption spectra for another set of parameters is shown in Figure 15. The excitonic spectra lie below 2.3 eV, the one-phonon vibronic spectra is in the region of 2.35–2.47 eV, and the two-phonon spectra are located in the region of 2.5–2.6 eV. It is curious to note the inverse mutual inversion of the more and the less intensive maxima of the red and green curves. The one-phonon vibronic spectra of the z-polarization exhibit three maxima as one can see in Figure 12.

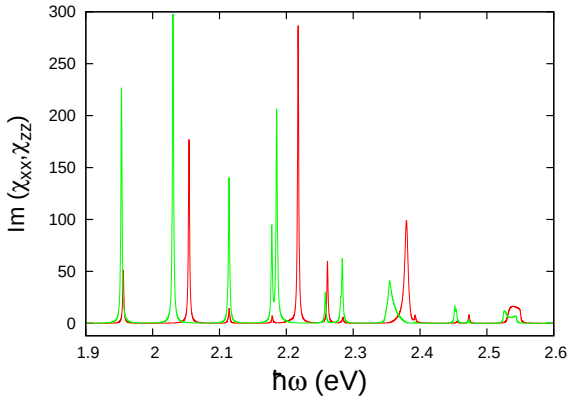

Figure 18. Linear absorption spectra in the case of strong exciton–phonon coupling ($\xi_{\mathrm{F}} = \xi = 1.1$). The values of other parameters are the same as in Figure 16.

Probably the additional splitting is a manifestation of a six-fold symmetry that is not the case of quadratic lattice (compare with Figure 7(a)).

The case of a weak exciton–phonon coupling is illustrated in Figure 16 ($\xi_{\mathrm{F}} = 0.6$, $\xi = 0.4$). The absorption is manifested in the excitonic region below 2.25 eV and in the one-phonon vibronic region only (above 2.25 eV). Owing to the weak exciton–phonon coupling, the vibronic spectra consist of many-particle continua located near the first vibronic replica of CTEs at 2.29 eV and near the first vibronic replica of the FE at 2.35 eV.

Figure 17 depicts again the case of "vibration on acceptors" ($\xi_{\mathrm{F}} = 0$). The excitonic spectra (Figure 17(a)) exhibit doublet structure in the (xy)-polarization and a weak maximum in the z-polarization. The one-phonon vibronics could be seen in the z-polarization solely and they exhibit two Lorentz-type maxima and a middle, not intensive continuum between them.

The opposite case of relatively strong exciton–phonon coupling can be seen in Figure 18. The absorption manifests itself in the excitonic region (below 2.09 eV), in the one-phonon vibronic region (2.1–2.23 eV), in the two-phonon vibronic spectra (2.23–2.39 eV), and even in the three-phonon region above 2.4 eV. In both cases – of quadratic and hexagonal lattices – the (xy)-polarization would be more expressed in the case of a strong coupling. We note the splitting of the absorption maximum near 2.18 eV, as well as the manifestation of wide continua in the two- and three-phonon spectra.

8 Conclusion and Outlook

In this study, we treat the well-known from Ising and Onsager's times model of a 2D quadratic lattice but instead of a set of magnetic moments we consider

a network of symmetrically located donor and acceptor molecules. The square and hexagonal symmetries facilitate considerations and govern the anisotropy of the model in the 2D lattice's plane and perpendicular to it. In our analytical calculations of the linear absorption, we touch the interaction of electromagnetic waves and excitons with transition dipole moments perpendicular to the lattice as well as the excitations polarized inside the lattice (x–y-models).

On the other hand, the essential feature of the two-component donor–acceptor system is the coupling of the excitations of a DA-pair (CTEs) and the collectivized excitations of one molecule (FEs). Our model reflects the transfers inside the systems of Frenkel and charge-transfer excitons and it includes the coupling between these two systems. Thus, our treatment can be interesting from a theoretical point of view and it may be useful in describing the excitonic and vibronic spectra of real materials. We stress here on the possibilities of the crystal engineering to produce layered and quasi two-dimensional materials of high symmetry.

The following results can be important in interpreting the excitonic and vibronic spectra of 2D (or quasi 2D) donor–acceptor systems:

— The FE–CTEs coupling can be very essential in an adequate description of absorption spectra – compare Figures 3 and 4 (without such a coupling) and Figures 6, 7, 12, 13, 17, and 18 (the coupling included).
— The natural anisotropy of 2D models (different properties inside the lattice plane and perpendicular to it) governs the FE–CTEs coupling terms, the transfer integrals, and respectively the excitonic and vibronic spectra.
— The cases in which a FE stems from donor and the intramolecular vibration is related with acceptor (or vice verse) must be considered very carefully. Owing to the absence of a FE–phonon coupling, the vibronic replicas of FEs are missing or they are very weak (see Figures 14 and 17).
— The six-fold symmetry of the hexagonal lattice can produce an additional splitting of the vibronic spectra observed in a quadratic lattice.
— The increasing number of vibrational quanta in the vibronic spectra is an obstacle in formation of one-particle exciton–phonon states. In our simulations, even two-phonon vibronics produce absorption corresponding to many-particle continua, not to Lorentz-type maxima.

Our model describes DA-systems with relatively high-mobility Frenkel and charge-transfer excitons. But the limitation of the model, as it is in other theories of vibronic spectra (see, e.g., [1], Ch. 3), is the assumption of weak resonant coupling compared with the energy of the vibrational quantum.

We do hope that our model of excitonic and vibronic spectra is an essential step toward successful studying the excitations in 2D and even 3D lattices of high symmetry.

Acknowledgments

The authors pay their tribute to the memory of Academician Christo Christov, a distinguished scientist and teacher. One of us, I.L., worked for a long period of time in activities of the Society of Physicists in Bulgaria under the presidency of Prof. Christov, and also as a Scientific secretary of the *Bulgarian Journal of Physics* together with Prof. Christov as an active member of the Editorial Board. The authors are indebted to Snezhana Yordanova for drawing Figures 1 and 10.

References

[1] V. M. Agranovich (2009) *Excitations in Organic Solids*, Oxford University Press, New York, chap. 3; see also (2003) *Thin Films and Nanostructures*, eds. V. M. Agranovich and G. F. Bassani, Elsevier, Amsterdam, chap. 6.

[2] D. Haarer (1974) *Chem. Phys. Lett.* (27) 91.

[3] D. Haarer, M. R. Philpott, and H. Morawitz (1975) *J. Chem. Phys.* **63** 5238.

[4] A. Brillante and M. R. Philpott (1980) *J. Chem. Phys.* **72** 4019.

[5] D. Haarer and M. R. Philpott (1983) in *Spectroscopy and Exciton Dynamics of Condensed Molecular Systems*, eds. V. M. Agranovich and R. M. Hochstrasser, North-Holland, Amsterdam, p. 27–82.

[6] W. Siebrand and M. Z. Zgierski (1983) in *Organic Molecular Aggregates*, eds. P. Reineker, H. Haken, and H. C. Wolf, Springer, Berlin, pp. 136–144.

[7] V. M. Agranovich and A. A. Zakhidov (1977) *Chem. Phys. Lett.* **50** 278.

[8] A. Elschner and G. Weiser (1985) *Chem. Phys.* **98** 465.

[9] H. Port and A. Hartschuh (2004) J. Lumin. **110** 315.

[10] G. Weiser (2004) *J. Lumin.* **110** 189.

[11] I. J. Lalov, C. Supritz, and P. Reineker (2008) *Chem. Phys.* **352** 1.

[12] I. J. Lalov, C. Warns, and P. Reineker (2008) *New J. Phys.* **10** 085006.

[13] L. Onsager (1944) *Phys. Rev.* **65** 117.

[14] T. L. Hill (1956) *Statistical Mechanics*, McGraw-Hill, New York.

[15] I.J. Lalov and I. Zhelyazkov (2012) *Bulg. J. Phys.* **39** 282.

[16] I.J. Lalov and I. Zhelyazkov (2013) *Chem. Phys.* **410** 71.

[17] N. M. R. Peres (2009) *Europhys. News* **40** 17.

[18] I. J. Lalov and I. Zhelyazkov (2007) *Phys. Rev.* B **75** 245435.

[19] R. W. Munn, P. Petelenz, and W. Siebrand (1987) *Chem. Phys.* **111** 207.

[20] A. S. Davydov (1971) *Theory of Molecular Excitons*, Plenum, New York.

[21] I. J. Lalov and I. Zhelyazkov (2013) *Chem. Phys.* **423** 127.

[22] M. Hoffmann, K. Schmidt, T. Fritz, V. M. Agranovich, and K. Leo (2000) *Chem. Phys.* **258** 73.

[23] L. Van Hove (1953) *Phys. Rev.* **89** 1189.